Desalination and Water Treatment
www.deswater.com
doi: 10.5004/dwt.2022.28692

268 (2022) 215–228
August

Effects of mooring configuration on the dynamic behavior of a TLP with tendon failure

Zhiyang Zhang[a], Minghao Du[a], Yanke Li[b], Weixing Liu[a], Haitao Wu[c,d,*], Lin Cui[e,*], Zhihu Yan[a], Xin Wang[a], Quanmi Liao[f], Meng Li[e]

[a]*School of Ocean Engineering, Jiangsu Ocean University, Lianyungang 222005, China*
[b]*State Key Laboratory of Mechanical System and Vibration, Shanghai Jiao Tong University, Shanghai 200240, China*
[c]*State Key Laboratory of Ocean Engineering, Shanghai Jiao Tong University, Shanghai 200240, China, email: 1600078087@qq.com (H. Wu)*
[d]*Collaborative Innovation Center for Advanced Ship and Deep-Sea Exploration, Shanghai 200240, China*
[e]*National Ocean Technology Centre, Tianjin 300112, China, email: cuilin_oceanenergy@126.com (L. Cui)*
[f]*School of Transportation and Environment, Shenzhen Institute of Information Technology, Shenzhen 518000, China*

Received 17 May 2022; Accepted 12 July 2022

ABSTRACT

In this paper, the dynamic behavior of a tension leg platform (TLP) in different mooring configurations with tendon failure was studied. After four different mooring configurations were determined, a fully coupled dynamic analysis program ANSYS/AQWA was used to develop a nonlinear hull-tendon numerical model. An effective method to simulate tendon failure was proposed, and six different failure conditions were identified. Under the regular wave, the influence of mooring configuration on the dynamic response and motion response spectrum of the platform under damaged mooring condition was investigated. The results show that the behavior of the platform in different mooring configurations are almost the same under intact mooring condition. However, under damaged mooring condition, the mooring configuration will cause the performance changes of the platform. In a certain mooring configuration, the dynamic response of the platform changes significantly with tendon failure. Therefore, the influence of tendon failure on the platform motion should be checked in advance to look for an optimal mooring configuration.

Keywords: Tension leg platform; Tendon failure; Mooring configuration; Dynamic behavior; Fully coupled dynamic analysis

1. Introduction

The tension leg platform (TLP) is a semi-compliant and semi-fixed offshore platform with a vertical mooring system. It produces much more buoyancy than gravity. In addition to offsetting its own weight, the remaining buoyancy balances the pretension provided by the tendons. With an increase of water depth, the load on the tendon increases significantly and the instability of the floating system enhances. Under extreme sea conditions, some tendons may fail due to overload. At the same time, local structural damage caused by accumulated fatigue, corrosion defects, installation damage, and accidental collisions may also cause mooring failure [1–3]. Tendon failure can change the performance of the floating system, which may affect the survivability of the platform. Some major organizations

* Corresponding authors.

have put forward a series of guidance documents and standards for mooring systems. They all require that a certain degree of redundancy should be considered to deal with the negative effects of mooring damage.

In the past years, the scholars have analyzed the dynamic behavior of various offshore structures when mooring damage occurs. Kim and Zhang [4] found that tendon failure of a TLP would cause accidental impact damage to the local structure at the connecting position, and proved that tendon failure at the top was more dangerous than that at the bottom. Yang and Kim [5] analyzed the impact of tendon failure on the dynamic response of a TLP's system, and compared the impact of tendon bottom failure and top failure. Gu et al. [6] specifically studied the effects of wave parameters on the dynamic behavior of TLP with tendon failure. Girón et al. [7] investigated the transient response of a FPSO with one mooring line failure in the harsh sea conditions. For symmetric and asymmetric mooring configurations, Ahmed et al. [8] studied the dynamic response of a truss spar platform after one or two mooring lines were disconnected. Through the coupling simulation of FAST and CHARM3D, Bae et al. [9] discussed the performance changes of a semi-submersible floating wind turbine with mooring line failure. A numerical model was developed to analyze the dynamic response of a TLP in the wave and current under intact and damaged mooring conditions [10]. Li et al. [11] developed a coupled aero-hydro-elastic numerical model to analyze the transient response of a spar platform with mooring line failure. Tabeshpour et al. [12] derived the stiffness matrix of a TLP under intact and damaged mooring conditions and established a numerical model to analyze its dynamic response with tendon failure. Ma et al. [13] used the time-domain analysis program SIMO to study the transient response of an OC4 DeepCwind semi-submersible floating wind turbine under typhoon conditions in the South China Sea. Le et al. [14] performed an aero-hydro-elastic-servo-mooring coupling analysis to analyze the hydrodynamic performance of a floating wind turbine with one mooring line failure. Yu et al. [15] compared the effects of simultaneous and continuous failure of multiple tendons on the dynamic behavior and tendon tension of a TLP under extreme sea conditions. Time-domain numerical simulations were used to analyze the hydrodynamic performance of a TLP with tendon failure [16]. In addition, sensitivity analysis was performed on the dynamic behavior of the TLP with different quantities of ballast. Chuang et al. [17] analyzed the transient response of a semi-submersible platform under mooring damaged conditions through a series of numerical simulations. With FAST, a coupled numerical model was developed to study the dynamic response of a TLP floating wind turbine with tendon failure [18]. Based on AQWA and FAST, a coupled code was developed to analyze the impact of mooring failure on the dynamic response of the rotor, platform and remaining mooring line of a barge floating wind turbine [19]. Qiao et al. [20] conducted a series of time-domain numerical simulations to evaluating the performance changes of a FPSO with different broken modes of mooring lines. A fully coupled dynamic analysis was carried out to study the performance changes of an engineering ship with mooring line failure [21]. Ren et al. [22] carried out a study on the design and hydrodynamic performance of a multi-column TLP-type wind turbine with several tendon failure scenarios. Zhang et al. [23] performed a series of numerical simulations to analyze the influence of mooring line failure on the dynamic behavior of a semi-submersible floating wind turbine.

Although the scholars mentioned above have done a lot of research on the dynamic behavior of various offshore structures under damaged mooring conditions, the influence of different mooring configurations on the platform performance under damaged mooring conditions is rarely involved [24]. In this paper, a hull-tendon nonlinear coupling model is established through the numerical simulation, and an effective method to simulate tendon failure is proposed. Then, the dynamic response and motion response spectrum of a TLP in different mooring configurations with one and two tendons failure are studied under the regular wave. The results have some reference value for the design and optimization of such mooring system.

2. Theoretical background

2.1. Potential flow theory

In this section, the hydrodynamic loads of diffracting structures in a regular wave are addressed. It is assumed that the velocity potential of the incident wave is zero. The fluid is ideal and irrotational, so the potential flow theory can be used. The wave velocity potential is as follows:

$$\varphi(x,y,z,t) = \varphi(x,y,z)e^{-i\omega t} \tag{1}$$

where φ is a complex potential function, which is divided into the radiation wave caused by the six modes of the floating structure motion, the incident wave and the diffraction wave. ω is the circular frequency of the incident wave. The velocity potential is very complex and can be divided into the following two parts [25].

- When a floating body moves in still water, the structure motion causes radiation. It's important to note that these forces are the functions of the structure motion. In addition, the mass coefficient and damping factor are considered in the dynamic equation.
- When the structure is assumed to be fixed in a regular wave, the wave excitation forces consists of two parts: Froud–Krylov force and diffraction force.

Therefore, the total velocity potential due to the incident wave of per unit amplitude can be expressed as:

$$\varphi(x,y,z)e^{-i\omega t} = \left(\varphi_I + \varphi_d + \sum_{j=1}^{6}\varphi_j x_j\right)e^{-i\omega t} \tag{2}$$

where φ_I is the incident potential, φ_d is the diffraction potential, φ_j is the radiation potential caused by the j-th motion, and x_j is the j-th motion under the per unit amplitude wave. The regular wave potential from linear theory can be expressed as follows:

$$\varphi = \frac{-ig\cosh\left[k\left(d+z\right)e^{ik\left(x\cos\theta+y\sin\theta\right)}\right]}{\omega\cos h\left(kd\right)} \tag{3}$$

where d, k and θ represents water depth, wave number and wave direction, respectively. By solving the Laplace equation, the potential function for the incompressible, non-viscous and irrotational fluid is obtained as follows:

$$\nabla^2\varphi = \frac{\partial^2\varphi}{\partial x^2} + \frac{\partial^2\varphi}{\partial x^2} + \frac{\partial^2\varphi}{\partial x^2} = 0 \tag{4}$$

At the same time, the following boundary conditions must be satisfied when the Laplace equation is solved [26].

Free surface boundary condition:

$$g\frac{\partial\varphi}{\partial z} - \omega^2\varphi = 0 \tag{5}$$

Bottom boundary condition:

$$\frac{\partial\varphi}{\partial z} = 0,\ z = 0 \tag{6}$$

Kinematic boundary condition:

$$\frac{\partial\varphi}{\partial n} = v\cdot n \tag{7}$$

Boundary condition at infinity:

$$\nabla\varphi = 0, r\to\infty, r = \sqrt{x^2+y^2+z^2} \tag{8}$$

where g is the acceleration of gravity, v is the velocity vector, and n is the surface normal vector.

2.2. Regular wave forces

The forces in each of the degree of freedom (DOF) can been estimated by integrating the pressure around the submerged or wet body surface [27].

$$F_j = -\int_{S_w} pn_j ds \tag{9}$$

where p is the fluid pressure, S_w is the wet body surface, and n is the normal direction.

Bernoulli's equation is generally used to calculate the fluid pressure acted on a floating body. For a hull system, this pressure is composed three parts, including the velocity filed, the hydrostatic and dynamic components [28]. So the unsteady pressure can be expressed as follows [29]:

$$p = -\rho\left(\frac{\partial\varphi}{\partial t} + \frac{1}{2}\left|\nabla\varphi\right|^2 - \frac{1}{2}u^2 + gz\right) \tag{10}$$

where u is the velocity of the point on the wet surface.

Therefore, the regular wave forces can be determined as:

$$F_j^r = -\rho g\iint_{S_w} zn_j ds - i\rho\omega A_{ij}e^{-\omega t}\iint_{S_w}\varphi_j n_j ds - i\rho\omega A_w e^{-\omega t}\iint_{S_w}\left(\varphi_I+\varphi_d\right)n_j ds \tag{11}$$

where A_{ij} is the displaced amplitude of the body and A_w is the amplitude of the regular wave.

The first term of Eq. (11) refers to the restoring force due to hydrostatic pressure. The second-term is the radiation force due to the body motion. The third component represents the exciting force component, which is the function of the incidence and diffraction wave potentials. The summation of the above three components is called the first-order wave force.

$$F_j^r = F_j^h + F_j^r + F_j^e \tag{12}$$

where F_j^h is the hydrostatic force, F_j^r is the radiation force, and F_j^e is the exciting force.

2.3. Tether model

The tendons adopts the tether model in this study [15]. They are considered as flexible cylindrical tubes whose diameters are small enough compared to the wavelength. The total force F_e applied on a tether element consists of three components:

$$F_e = F_w + F_s + F_d \tag{13}$$

where F_w, F_s and F_d are the gravity, hydrostatic force, and hydrodynamic force, respectively.

According to the Morrison's theory, the hydrodynamic force acting on the tendon can be expressed as [30]:

$$F_d^n = \frac{1}{2}C_D\rho A\left(u-v_t\right)\left|u-v_t\right| + \frac{\pi}{4}C_M\rho A^2\dot{u} - \frac{\pi}{4}C_A\rho A^2\dot{v}_t \tag{14}$$

where C_D is the drag force coefficient of the tendon element; $C_M = C_A + 1$ is the inertial force coefficient; C_A is the added mass coefficient; ρ is the density of seawater; v_t is the velocity of the tether element; A is the equivalent diameter of the tether element; $\dot{u}$ is the incoming flow acceleration.

2.4. Equation of motion

The TLP is divided into multiple panels and Morison elements, and its equation in the frequency domain can be expressed as follows [31]:

$$\left[-\omega^2\left(M_s+M_a\right) - i\omega C + K\right]X\left(j\omega\right) = F\left(j\omega\right) \tag{15}$$

where M_s is the total structural matrix, and M_a is the total added mass matrix. C and K are the total damping and stiffness matrix, respectively. $F(j\omega)$ represents the wave excitation force.

In the time domain, the platform can be regarded as a rigid body subjected to constraints and external forces. Its motion equation can be written as:

$$\left(M+A_{\infty}\right)\ddot{x}(t)+\int_0^t R(t-\tau)\dot{x}(\tau)d\tau+Kx(t) = F_w(t)+F_m(t)+F_d(t) \quad (16)$$

where M is the mass matrix; A_{∞} is the added mass matrix at infinite frequency; $x(t)$ is the displacement vector; $\int_0^t R(t-\tau)\dot{x}(\tau)d\tau$ is the radiation damping force, $R(t)=\frac{2}{\pi}\int_0^{\infty}\left[A(\omega)-A_{\infty}\right]\cos\omega t d\omega$ is the retardation function, $A(\omega)$ is the added mass matrix at the circular frequency ω [32]; K is the hydrostatic restoring matrix; $F_w(t)$ represents the regular wave forces; $F_m(t)$ is the coupling force between tendons and platform; $F_d(t)=0.5\rho C_{dh}A_h\left(u-\dot{x}_h\right)\left|u-\dot{x}_h\right|$ refers to the viscous damping force acting on the Morrison elements (columns and pontoons) [33], where C_{dh} is the viscous damping coefficient, A_h is the equivalent diameter of the Morrison element, u is the incoming flow velocity, and $\dot{x}_h$ is the platform velocity.

3. Numerical simulation

3.1. Numerical tool

ANSYS/AQWA is widely used to analyze the hydrodynamic performance of a floating system. This program can consider the coupling between the platform motion and mooring line dynamics. The hydrodynamic coefficients, including added mass, radiation damping and wave exciting force transfer functions, can be obtained from the frequency-domain module [34]. The obtained hydrodynamic coefficients are transformed into the time-domain form by Fourier transform (FT) and convolution integral technique (CIT), and then transferred to the time-domain module as the external force input of the platform. Fig. 1 shows the flow chart of the numerical simulation in this paper.

3.2. Simulation of tendon failure

Since AQWA has no in-house code to achieve tendon failure, an effective method is proposed in this paper. This method can be divided into five steps: First, the platform is simulated in the time domain under intact mooring condition; Second, export the tension time history of the specified tendon, and extract the data from the initial time to the failed time. Third, the extracted data is recompiled into the external force input file, which is readable by the time-domain module. Fourth, after removing the specified tendon and inputting the external force file, the simulation is carried out again. Fifth, the results are obtained by solving the damaged mooring condition.

The program can only output tendon tension, but the readable external force file for the time-domain simulation requires six DOFs load data. Next, the process how to obtain six DOFs load data through tendon tension is introduced. Fig. 2 shows a schematic diagram of a floater in motion.

Where $\vec{R}$ is the distance vector from the center of gravity to the fairlead, $\vec{T}$ is the tendon tension vector, L is the tendon length, h is the water depth, l is the projection length of the tendon in the x-axial direction, w is the projection length of the tendon in the y-axial direction, and f is the projection length of the tendon in the z-axial direction.

The coordinate system in Fig. 2 is the global coordinate system. It is assumed that $P_N = (x_N, y_N, z_N)$ is the position of the node N, $P_1 = (x_1, y_1, z_1)$ is the position of node 1, P_G (x_g, y_g, z_g) is the position of the center of gravity, $\vec{T}=\left(T_x,T_y,T_z\right)$ is the component expression of tendon tension, and T is the magnitude of tendon tension. Therefore:

$$f = h + z_N \quad (17)$$

$$w = \left|y_N - y_1\right| \quad (18)$$

$$l = \left|x_N - x_1\right| \quad (19)$$

$$\vec{R} = P_N - P_G = \left(x_N - x_g, y_N - y_g, z_N - z_g\right) \quad (20)$$

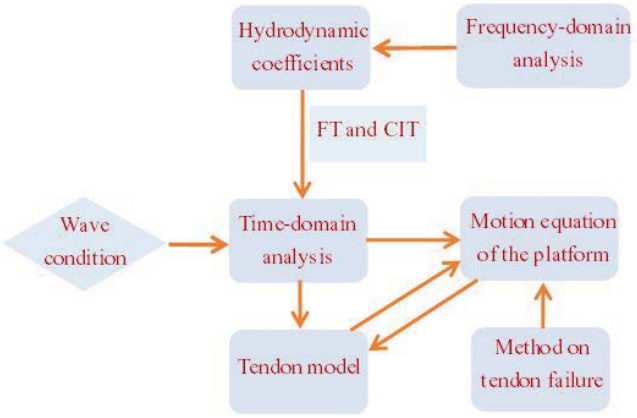

Fig. 1. Flow chart of the numerical simulation.

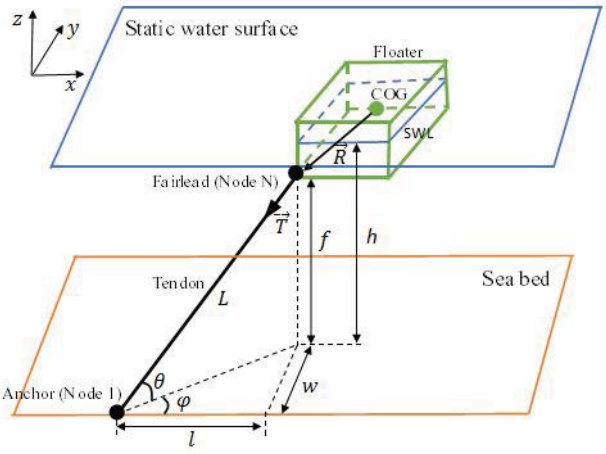

Fig. 2. Schematic diagram of the floater in motion.

$$\sin\theta = \frac{f}{L} \tag{21}$$

$$\cos\theta = \sqrt{1-\left(\frac{f}{L}\right)^2} \tag{22}$$

$$\cos\varphi = \frac{l}{\sqrt{l^2+w^2}} \tag{23}$$

$$\sin\varphi = \frac{w}{\sqrt{l^2+w^2}} \tag{24}$$

Then, the dynamic system in Fig. 2 is analyzed mechanically:

$$T_x = -T\cos\theta\cos\varphi \tag{25}$$

$$T_y = -T\cos\theta\sin\varphi \tag{26}$$

$$T_z = -T\sin\theta \tag{27}$$

In addition, the bending moment caused by tendon tension is:

$$\vec{M} = \vec{R}\times\vec{T} \tag{28}$$

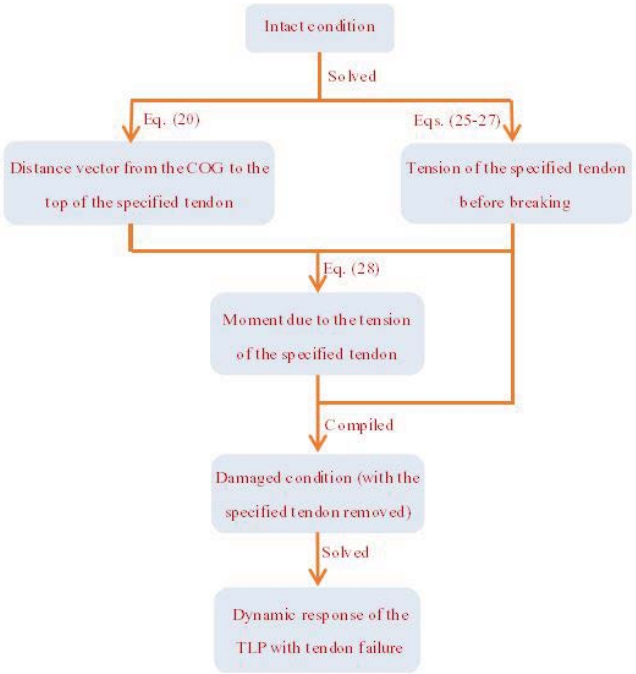

Fig. 3. Procedure of tendon failure.

Finally, the load data of six DOFs obtained from tendon tension can be expressed as $\left[\vec{T},\vec{M}\right]$.

In order to better demonstrate how this paper simulates tendon failure, Fig. 3 gives the procedure as the flow chart.

4. TLP system and tendon failure conditions

The TLP consists of one deck, four column and four pontoons. It's geometrically symmetric. To ensure the safety of the platform, eight tendons anchor it to the seabed. Table 1 describes the parameters of the TLP system. This paper studies the dynamic behavior of the TLP with one or two tendons failure in different mooring configurations. Fig. 4 presents four different mooring configurations (MCs). The difference lies in the tendon interval angle.

Table 1
Parameters of the TLP system

Parameter	Value
Displacement (t)	43,000
Draft (m)	28.5
Diameter of column (m)	19
Height of pontoon (m)	7.3
Width of pontoon (m)	9.5
Distance between columns (m)	55
Center of gravity height (from the kneel) (m)	38.25
Radius of gyration R_{xx} (m)	32.3
Radius of gyration R_{yy} (m)	32.3
Radius of gyration R_{zz} (m)	29.2
Length of tendon (m)	308.65
External radius of tendon (mm)	960
Axial stiffness of tendon (N)	2.03E+10
Bending stiffness (N/m^2)	2.20E+09
Pretension of tendon (t)	1,300
Water depth (m)	330

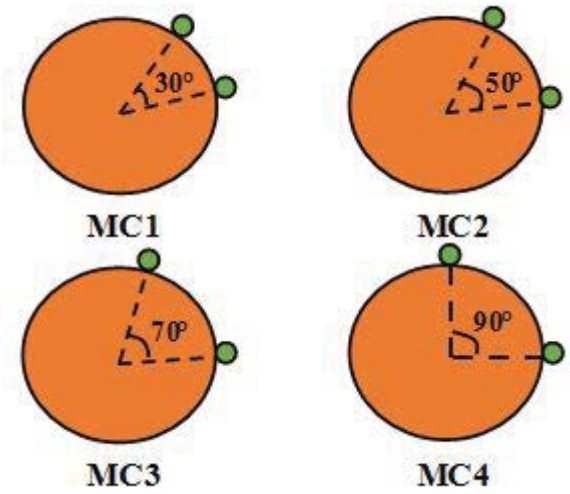

Fig. 4. Four different mooring configurations.

A regular wave is selected to simulate the performance changes of the TLP with tendon failure. The wave height is 8 m, the period of 10 s, and the incident direction is 45°. Fig. 5 shows a schematic diagram of the platform under the regular wave. In the figure, θ indicates the incident direction of the wave. In general, a TLP is designed to not survive from the loss of 3 or more tendons. Due to the wave incident direction, #3, #5, #6 and #8 are likely disconnected. Therefore, six different tendon failure conditions are selected, namely, #3 failure, #5 failure, #3#5 failure, #3#6 failure, #3#8 failure and #5#6 failure. In addition, one tendon failure causes the tension level of the remaining tendon to increase rapidly in a short time, which will leads to the progressive failure. When the progressive failure of two tendons occurs over a short period of time, it can be considered simultaneous, which is extremely dangerous. Therefore, under damaged mooring condition, the selected two tendons fail simultaneously.

5. Results and discussions

This paper studies the dynamic behavior of the TLP in different MCs with one or two tendons failure. In order to obtain accurate simulation results, a fully coupled time-domain dynamic analysis program is used to analyze the platform's motion performance. The simulation time of each case is 600 s and the time step is 0.1 s. To avoid the influence of the initial transient effect, the selected tendon is disconnected when the platform enters a steady phase. The failed time is at 183 s, when the tendon is at the maximum tension. When the specified tendon is disconnected, the force at the connection between the tendon and the hull immediately becomes zero. The analysis on the platform motion with tendon failure mainly focuses on the 3° of freedom (DOFs): surge, heave and pitch. The motion response spectrum of the platform is obtained from the dynamic response at the steady phase with tendon failure through fast Fourier transform (FFT).

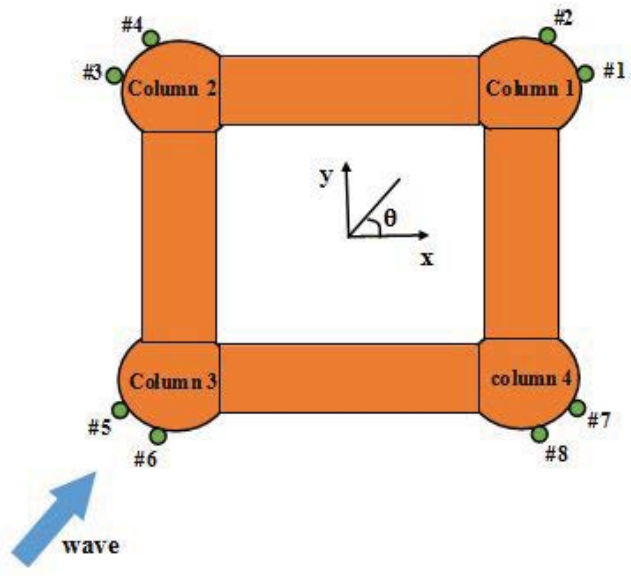

Fig. 5. Schematic diagram of the TLP under the wave condition.

5.1. Dynamic response with tendon failure

It can be seen from Fig. 6a that when #3 fails, the surge motion does not experience a transient response, which means that #3 failure has no effects on the surge response. The surge restoring stiffness is low due to small angle between vertical plane and inclined tendon with intact tendon, so one tendon failure cannot result a significant change in the surge motion. At the same time, the surge response in different MCs is the same. It can be observed from Fig. 6b that under intact and damaged mooring conditions, the heave response in different MCs is the same. After #3 fails, the platform experiences a transient response of 0.088 m in the heave direction. The transient phase lasts for 21 s. The average response in steady phase increases by 90.00% compared with that in the initial phase, while the standard deviation (STD) increases by 7.08%. This means that #3 failure results in a weakening of the heave restoring stiffness. It can be seen from Fig. 6c that the pitch motion of the platform is almost the same under intact mooring condition. After #3 fails, the pitch motion in different MCs experiences different transient responses. The transient phase also lasts for 21 s. Moreover, the transient response increases with an increase of tendon interval angle. The transient response in MC4 is 17.22% larger than that in MC1. In the steady phase, the pitch response also increases with an increase of tendon interval angle. This is because the smaller the angle between #3 and the longitudinal section of the platform, the greater its contribution to the pitch restoring stiffness. The average response in MC4 is 13.23% larger than that in MC1, while the STD increases by 15.19%. In addition, the average response in the steady phase in MC4 increases by 0.075° compared with that in the initial phase, while the STD increases by 12.98%. This indicates that the pitch restoring stiffness decreases with #3 failure.

It can be inferred from Fig. 7 that the influence of #5 failure on the platform motion is similar to that of #3 failure. #5 failure does not change the surge response, while it decreases the heave and pitch restoring stiffness significantly. The dynamic response of the surge and heave motions is the same in different MCs. However, with an increase of tendon interval angle, the dynamic response of the pitch motion increases in steady phase. This is because the smaller the angle between #5 and the longitudinal section, the greater its contribution to the pitch restoring stiffness.

It can be seen from Fig. 8a that the surge motion is not affected by the transient effect, which means that #3#5 failure does not affect the surge response. It can be observed from Fig. 8b that when #3#5 fail, the heave motion undergoes a large transient response. The transient phase lasts for 30 s. The transient response increases with an increase of tendon interval angle. The transient response in MC4 is 23.55% larger than that in MC1. Similarly, the dynamic response of steady phase increases with an increase of tendon interval angle. The average heave response in MC4 is 18.18% larger than that of MC1, while the STD increases by 4.52%. In addition, the average response of the steady phase in MC4 is 0.105 m larger than that in the initial

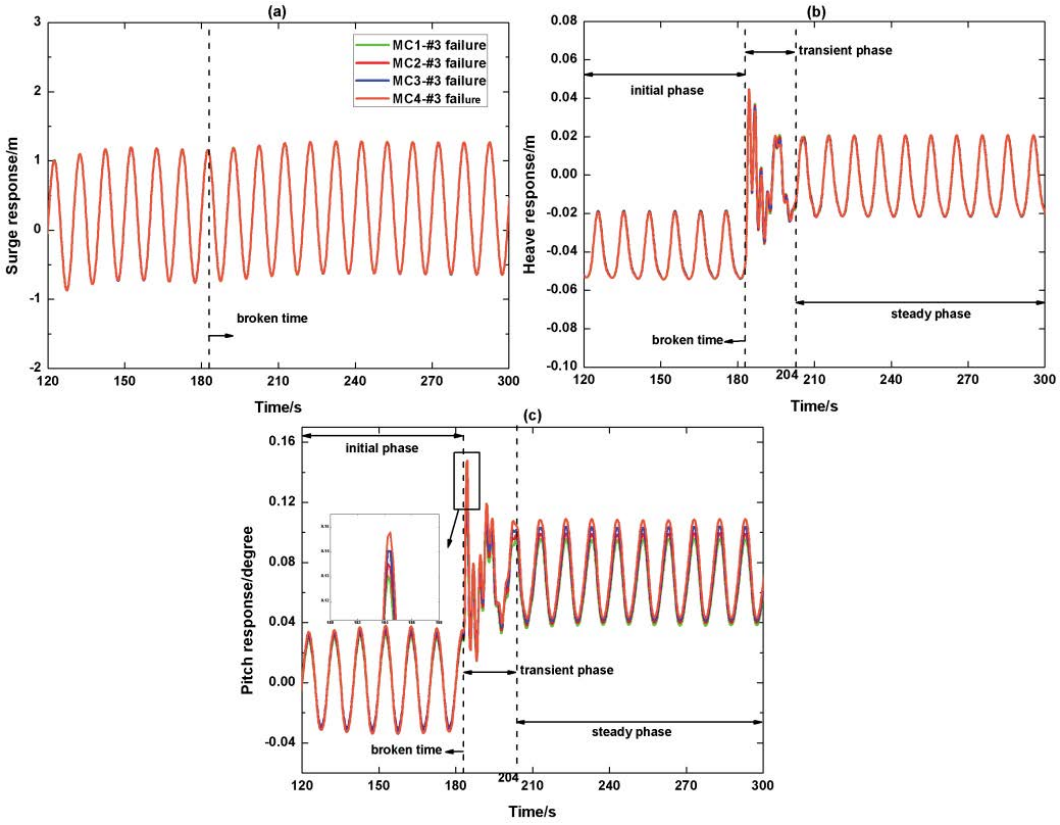

Fig. 6. Dynamic response with #3 failure.

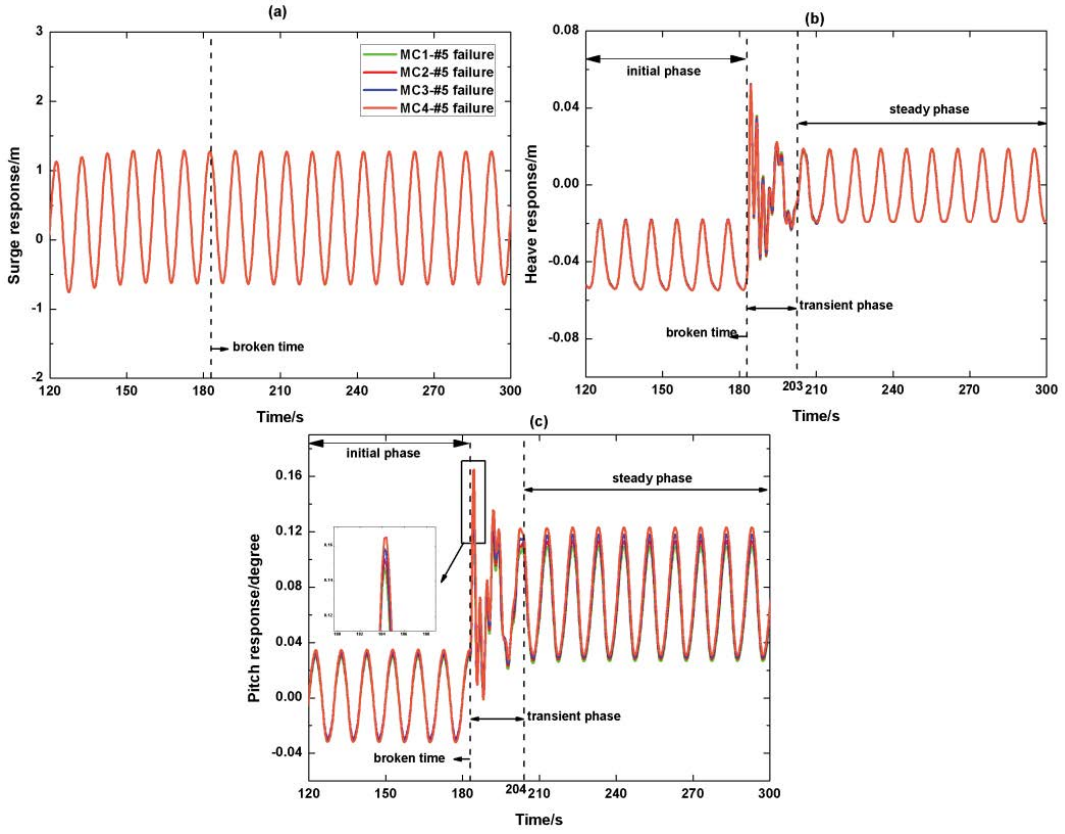

Fig. 7. Dynamic response with #5 failure.

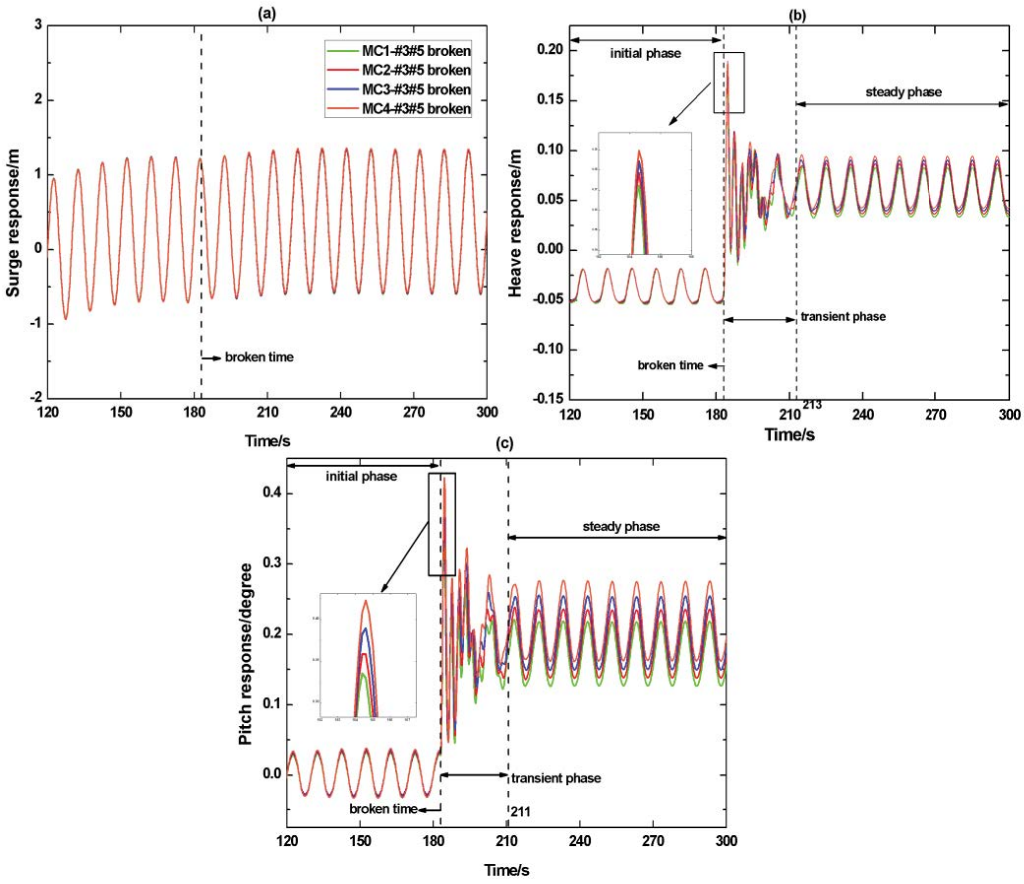

Fig. 8. Dynamic response with #3#5 failure.

stage, while the STD increases by 45.67%. It can be inferred from Fig. 8c that the influence of #3#5 failure on the pitch motion is similar to that on the heave motion. The transient phase lasts for 28 s. The transient response in MC4 is 29.17% larger than that in MC1. The average pitch response of steady phase in MC4 is 26.58% larger than that in MC1, while the STD increases by 23.53%. In addition, the average response of the steady phase in MC4 is 0.215° larger than that in the initial stage, while the STD increases by 46.31%.

After #3#5 fail, the dynamic response of the heave and pitch motions increases with an increase of tendon interval angle. This is because the smaller the angle between #3#5 and the longitudinal section, the greater their contribution to the heave and pitch restoring stiffness.

As can be seen from Fig. 9a, #3#6 failure does not change the surge response. Moreover, the surge response in different configurations is the same. It can be observed from Fig. 9b, c that after #3#6 fail, both heave and pitch motions undergo a transient phase of 28 s, and the maximum transient response in different MCs is consistent. The maximum transient response of the heave motion is 0.202 m, while that of the pitch motion is 0.269°. When the platform enters the steady phase, the heave response in different MCs is the same, as is the pitch response. In addition, the dynamic response in the steady phase is much larger than that in the initial phase. The average response of the heave and pitch DOFs in the steady phase is 0.09 m and 0.153° larger than those in the initial phase, respectively, while the STDs increases by 36.22% and 47.11%, respectively.

It can be inferred from Fig. 10a and b that the influence of #3#8 failure on the surge and heave motions is similar to #3#6 failure. The surge response does not change with #3#8 failure, but the heave restoring stiffness is significantly reduced. The dynamic response of the surge motion in different MCs is the same, and so is the heave motion. However, it can be observed from Fig. 10c that the dynamic response of the pitch motion increases with an increase of tendon interval angle with #3#8 failure. The average pitch response in MC4 is 0.011° larger than that in MC1, while the STD increases by 10.52%. This is because the smaller the angle between #3 and the longitudinal section, the greater its contribution to the pitch restoring stiffness. In addition, from the above analysis of other damaged mooring conditions, it can be inferred that the pitch motion will have a significant transient response regardless of one tendon failure or two tendons failure. However, it can be seen from Fig. 10c that the transient response is not significant after #3#8 fail. This is because the vertical stiffness of the bow and stern will not differ significantly with #3#8 failure.

It can be seen from Fig. 11a that after #5#6 fail, the platform's surge motion in different MCs experiences a transient response to some extent. This indicates that, different from

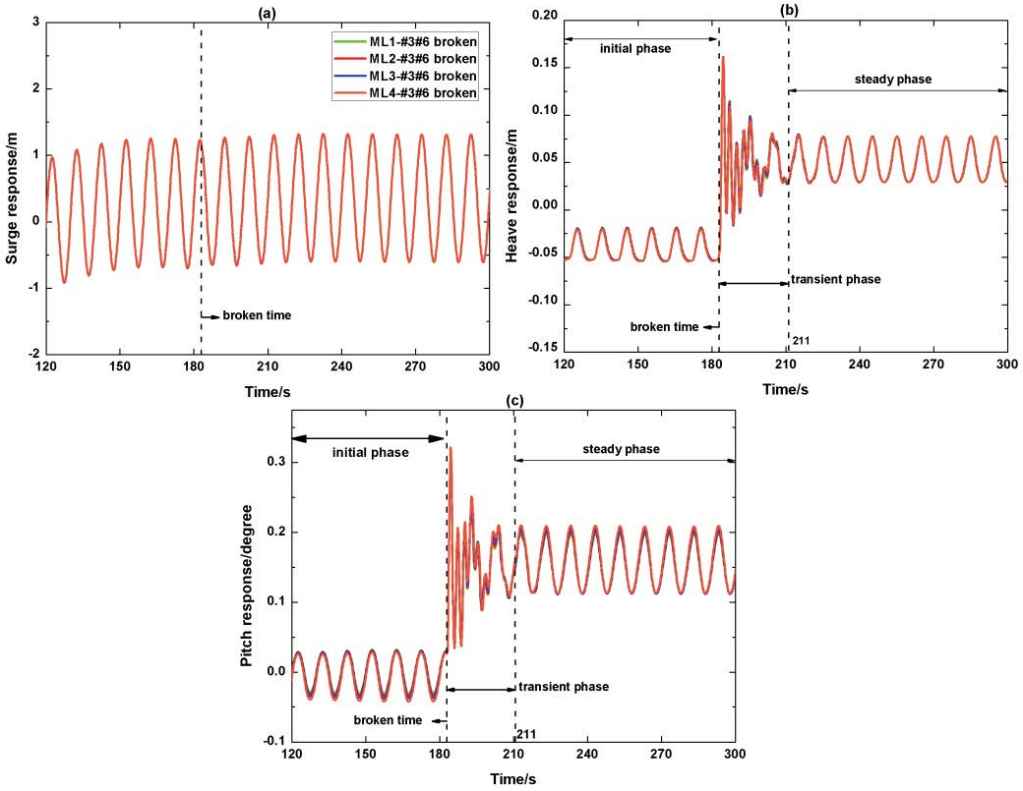

Fig. 9. Dynamic response with #3#6 failure.

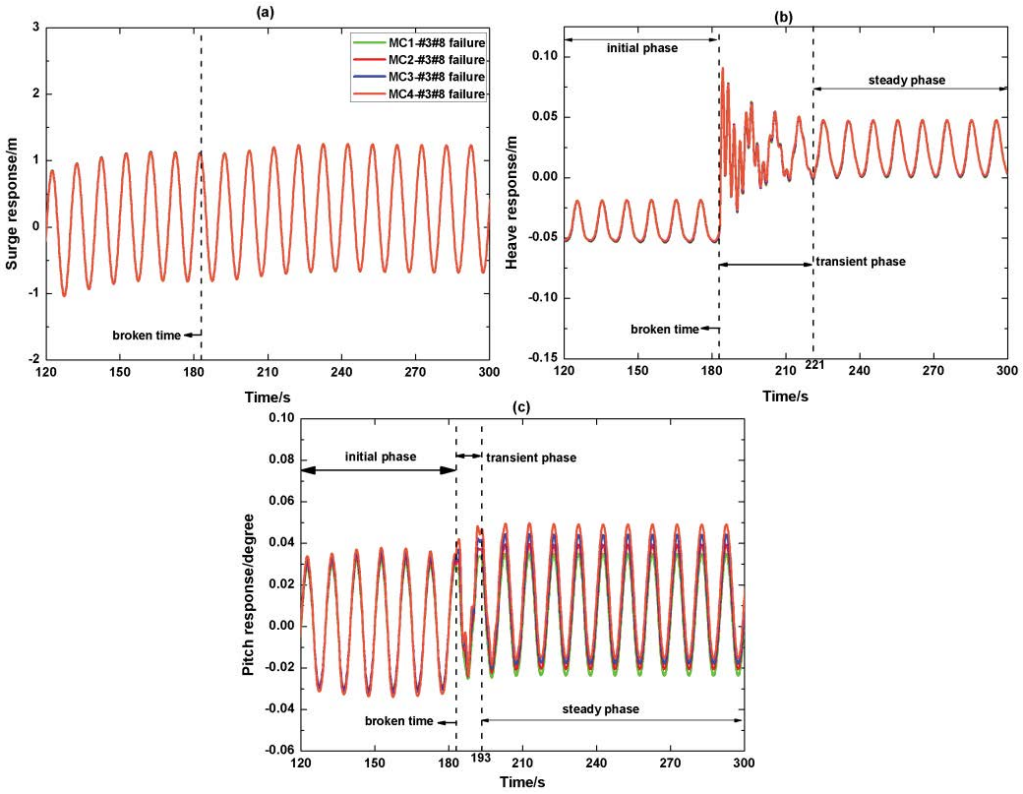

Fig. 10. Dynamic response with #3#8 failure.

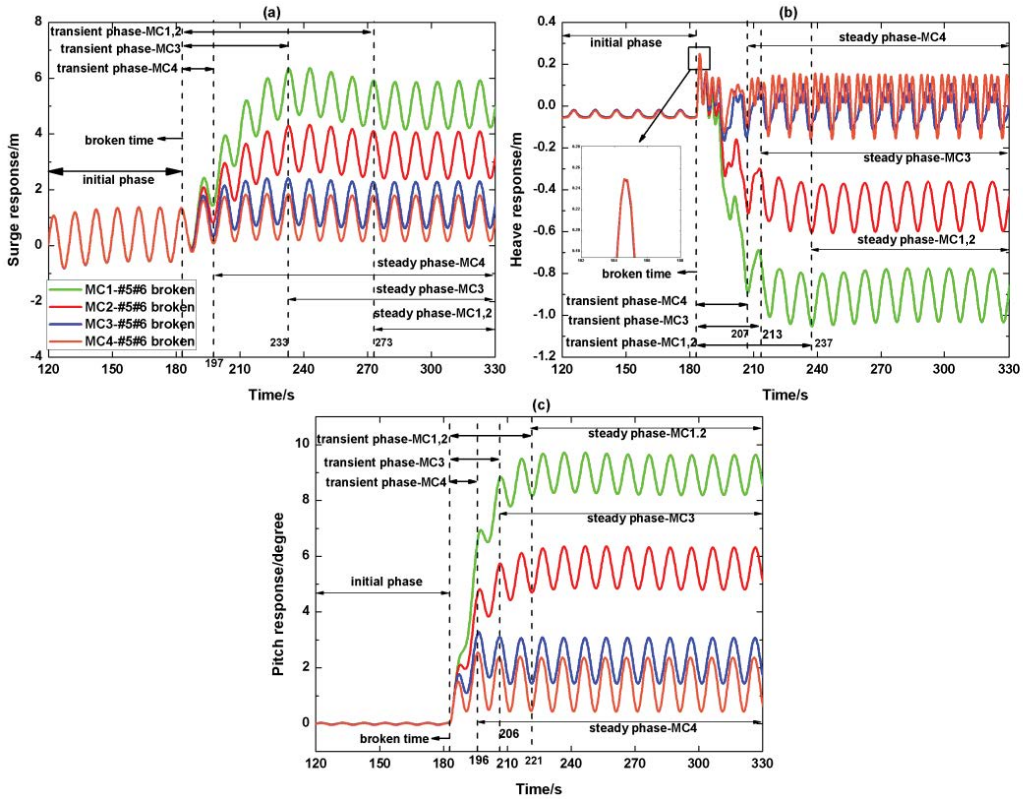

Fig. 11. Dynamic response with #5#6 failure.

other damaged mooring conditions, the reduction in the surge stiffness due to #5#6 failure is enough to change the response significantly, while the surge stiffness is low with intact tendon. With an increase of tendon interval angle, the surge transient response decreases. This is because the larger the tendon interval angles, the larger the restoring stiffness of the remaining tendons to the surge motion. The maximum response of the transient phase in MC1 is 6.356 m, which is 4.501 m larger than that in MC4. Moreover, the larger the tendon interval angle, the shorter the transient phase lasts. For example, the transient phase in MC4 lasts only 17 s, 76 s less than those in MC1 and MC2. When the platform enters the steady phase, the dynamic response of the surge motion decreases with an increase of tendon interval angle. The average response in MC1 is 4.093 m larger than that in MC4, while the STD increases by 4.10%. In addition, it can be seen from Fig. 11a that the surge motion does not reach the maximum transient response immediately after #5#6 fail, which indicates that the transient effect has a certain delay. It can be observed from Fig. 11b that after the #5#6 fail, the heave motion immediately undergoes a transient response, and the maximum response in the transient stage is the same in different MCs. MC1 and MC2 have the longest transient phase, while MC4 has the shortest transient phase. When the platform enters the steady phase, the dynamic response of the heave motion increases obviously. Moreover, the smaller the tendon interval angle, the larger the dynamic response. The average heave response in MC1 is 0.932 m larger than that in MC4, but the STD is almost the same. It is noteworthy that the dynamic response of the steady phase in MC3 and MC4 has high-frequency components. This makes the non-linearity of the heave motion apparent. The heave response in MC1 and MC2 is significantly larger than that in MC3 and MC4, which is attributed to the significant set-down of the platform rather than the significant reduction in the heave restoring stiffness. It can be inferred from Fig. 11c that #5#6 failure has a similar influence on the pitch motion as the surge motion. However, there is also a difference, that is, the maximum response in MC1 and MC2 does not appear in the transient phase, but in the steady phase.

It can be seen from Fig. 11 that #5#6 failure will have a significant impact on the platform motion in MC1 and MC2, compared with other MCs. It can be inferred that if MC1 or MC2 is adopted, the safety of the platform will be seriously threatened after #5#6 fail.

In order to better demonstrate the influence of different MCs on the performance of TLP with tendon failure, Fig. 12 gives the mean value and STD of the platform motions under intact and damaged mooring conditions. The results of the platform motions with tendon failure appear in the steady phase. In this figure, the column represents the mean value, and the error bar represents the STD.

5.2. Motion response spectrum with tendon failure

In the last section, the influence of tendon failure in different MCs on the dynamic response of the platform has been analyzed. This section discusses the influence of tendon failure on the motion response spectrum. The analysis objects are mainly focused on the DOFs, of which the

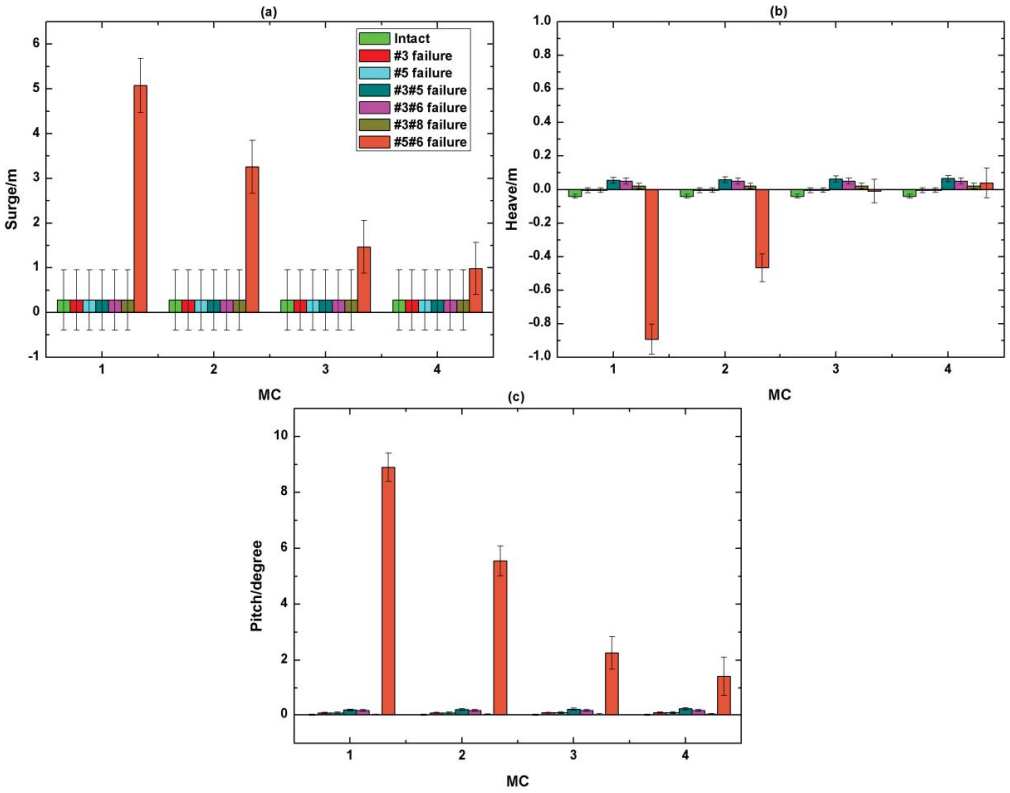

Fig. 12. Mean value and STD of the platform motions.

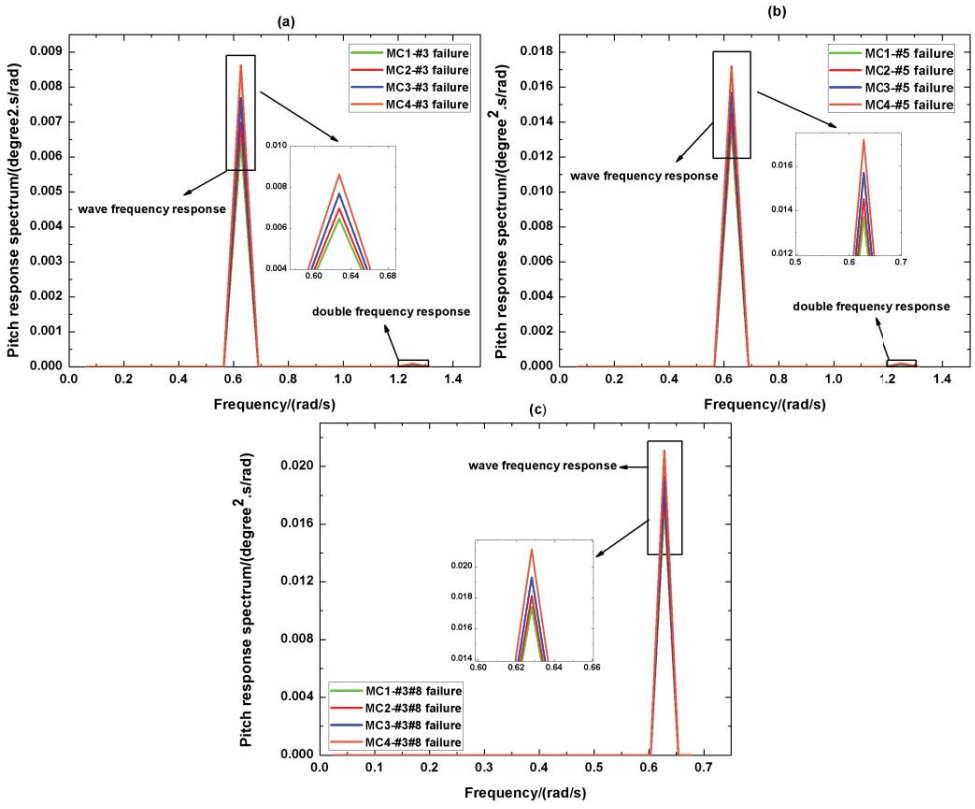

Fig. 13. Pitch response spectrum with #3, #5, and #3#8 failure.

dynamic response changes in different MCs, including the pitch motion with #3, #5, and #3#8 failure, the heave and pitch motions with #3#5 failure, and three motions with #5#6 failure.

It can be seen from Fig. 13 that under the conditions of #3, #5 and #3#8 failure, the wave frequency response of the pitch response spectrum increases with an increase of tendon interval angle. This means that the larger the tendon interval angle, the larger the oscillating amplitude of the pitch motion. In addition, under the conditions of #3 and #5 failure, there is a double frequency component in the response spectrum, but the proportion is significantly small.

It can be observed from Fig. 14a that there are wave frequency and double frequency responses in the heave response spectrum, but the wave frequency component is dominant. Moreover, the heave response spectrum does not change with the change of tendon interval angle. It can be seen from Fig. 14b that the wave frequency response increases with an increase of tendon interval angle. Under this mooring damaged condition, the oscillation amplitude of the heave motion in different MCs is the same, but the oscillation amplitude of the pitch motion increases with an increase of tendon interval angle.

It can be seen from Fig. 15a that the wave frequency component of the surge response spectrum does not change with the variation of tendon interval angle, indicating that the oscillating amplitude of the surge motion in different MCs remains unchanged. It can be observed from Fig. 15b

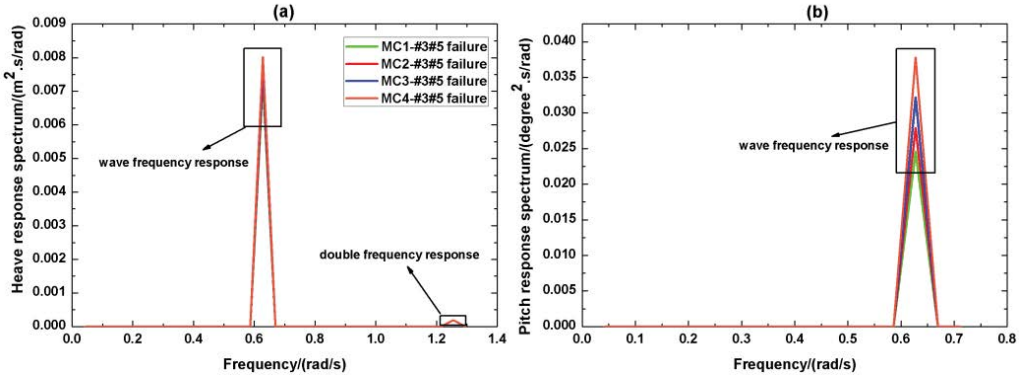

Fig. 14. Heave and pitch response spectrum with #3#5 failure.

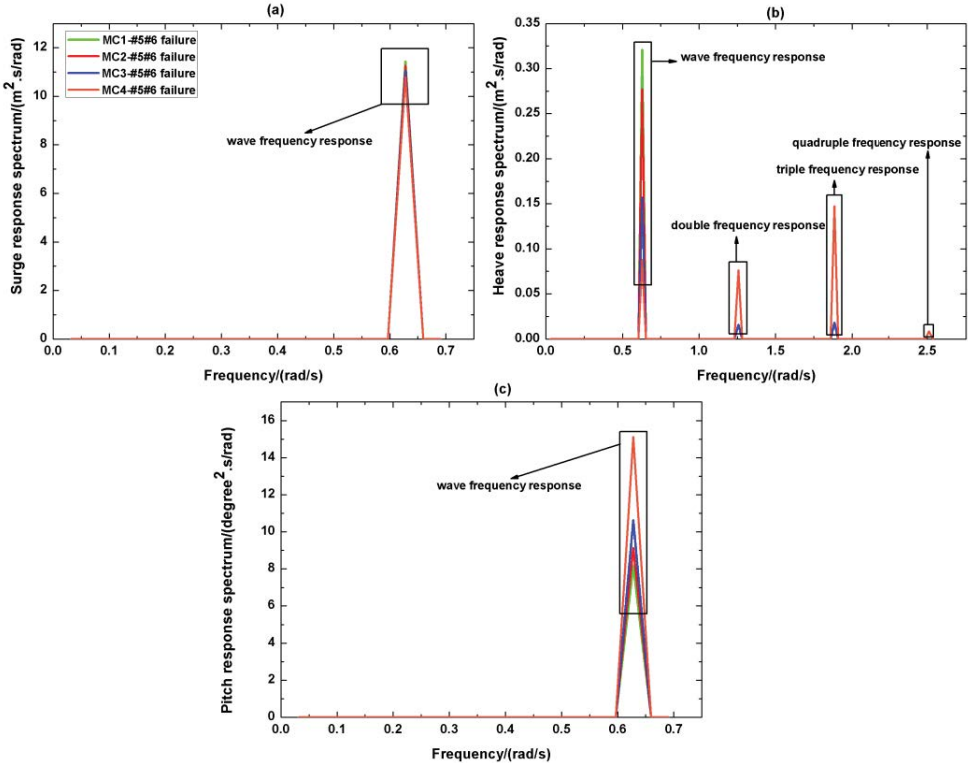

Fig. 15. Motion response spectrum with #5#6 failure.

that due to the strong nonlinearity after #5#6 fail, the heave response spectrum in MC4 contains wave frequency, double frequency, triple frequency and quadruple frequency components. The wave frequency response is the maximum and the quadruple frequency response is the minimum. The double and triple frequency responses account for a relatively large proportion in the heave response spectrum. In MC3, the heave response spectrum consists of wave frequency, double frequency and triple frequency components, among which the wave frequency response plays a dominant role. In MC1 and MC2, only wave frequency component exists in the heave response spectrum. At the wave frequency, the heave response decreases with an increase of tendon interval angle. However, on the whole, the oscillating amplitude of the heave motion is the largest in MC4. In addition, except for MC4, the oscillating amplitude of the heave motion decreases with an increase of tendon interval angle. It can be seen from Fig. 15c that the wave frequency response increases with an increase of tendon interval angle. This indicates that the larger the tendon interval angle, the larger the oscillating amplitude of the pitch motion.

6. Conclusions

In the present study, the motion performance of a TLP in different MCs with one or two tendons failure is investigated. To consider the coupling between the hull and tendons, a fully coupled dynamic analysis program is used. To obtain the dynamic response with tendon failure, an effective method is proposed to simulate the failure of a specified tendon at a certain time. After a series of time domain simulations, the following conclusions can be drawn:

- Under intact tenon condition, the platform motion in different MCs is almost the same.
- The heave and pitch responses with tendon failure increase due to the reduction in restoring stiffness. However, the surge response only increases with two tendons failure in one column.
- After two tendons in one column fail, the dynamic response decreases significantly with an increase of the tendon interval angle.

This study is helpful to understand the influence of mooring configuration on the dynamic behavior of a TLP with tendons failure, and has some reference value for the design and optimization of such mooring system.

Declaration of competing interest

The authors declare that they have no known competing financial interests or personal relationships that could have appeared to influence the work reported in this paper.

Acknowledgement

This work is supported by National Natural Science Foundation of China (Grant Nos. 52001138; 52101356), National Natural Science Foundation of Jiangsu Province (Grant No. BK20201029), National Science Foundation of the Jiangsu Higher Education Institutions of China (Grant Nos. 20KJB416005; 21KJB580011) and Guangdong Provincial General Colleges and Universities Yong Innovative Talents Project (Grant No. 2020KQNCX207).

References

[1] K.T. Ma, H. Shu, P. Smedley, D. L'Hostis, A. Duggal, A Historical Review on Integrity Issues of Permanent Mooring Systems, Offshore Technology Conference, Texas, USA, 2013.
[2] R.B. Gordon, M.G. Brown, E.M. Allen, Mooring Integrity Management: A State-of-the-art Review, Offshore Technology Conference, Texas, USA, 2014.
[3] I. Prislin, S. Maroju, Mooring Integrity and Machine Learning, Offshore Technology Conference, Texas, USA, 2017.
[4] M.H. Kim, Z. Zhang, Transient effects of tendon disconnection on the survivability of a TLP in moderate-strength hurricane condition, Int. J. Nav. Archit. Ocean Eng., 1 (2009) 13–19.
[5] C.K. Yang, M.H. Kim, Transient effects of tendon disconnection of a TLP by hull-tendon-riser coupled dynamic analysis, Ocean Eng., 37 (2010) 667–677.
[6] J.Y. Gu, Y. Chen, P.T. Geng, W.M. Liu, Study on the dynamic response and tension characteristics of a TLP with one tendon broken, J. Ship Mech., 19 (2015) 1488–1497.
[7] A.R.C. Girón, B.W. Kim, J.A.M. Farfán, A.O.V. Hernández, Transient Effects of an FPSO With a Broken Mooring Line, Proceedings of 25th International Ocean and Polar Engineering Conference, Kona, Big Island, Hawaii, USA, 2015.
[8] M.O. Ahmed, A. Yenduri, V.J. Kurian, Evaluation of the dynamic responses of truss spar platforms for various mooring configurations with damaged lines, Ocean Eng., 123 (2016) 411–421.
[9] Y.H. Bae, M.H. Kim, H.C. Kim, Performance changes of a floating offshore wind turbine with broken mooring line, Renewable Energy, 101 (2017) 364–375.
[10] D.O. Oyejobi, M. Jameel, H.R. Sulong, Stochastic response of intact and a removed tendon tension leg platform to random wave and current forces, Arabian J. Sci. Eng., 42 (2017) 1065–1076.
[11] Y. Li, Q. Zhu, L.Q. Liu, Y.G. Tang, Transient response of a SPAR-type floating offshore wind turbine with fractured mooring lines, Renewable Energy, 122 (2018) 576–588.
[12] M.R. Tabeshpour, A. Ahmadi, E. Malayjerdi, Investigation of TLP behavior under tendon damage, Ocean Eng., 156 (2018) 580–595.
[13] G. Ma, L. Zhong, Q.W. Ma, Y.W. Zhu, H.W. Wang, Dynamic Analysis of Mooring Break for a Semi-Submersible Floating Offshore Wind Turbine, The 29th International Ocean and Polar Engineering Conference, Hawaii, USA, 2019.
[14] C. Le, Y. Li, H. Ding, Study on the coupled dynamic responses of a submerged floating wind turbine under different mooring conditions, Energies, 12 (2019) 418, doi: 10.3390/en12030418.
[15] J.X. Yu, S. Hao, Y. Yu, B.Q. Chen, S.Y. Cheng, J.Y. Wu. Mooring analysis for a whole TLP with TTRs under tendon one-time failure and progressive failure, Ocean Eng., 182 (2019) 360–385.
[16] Y.H. Qi, X.L. Tian, X.X. Guo, H.N. Lu, L. Liu, The hydrodynamic performance of a tension leg platform with one-tendon failure, Ships Offshore Struct., 14 (2019) 523–533.
[17] Z.J. Chuang, X. Chang, C.Z. Li, Y. Lu, S.W. Liu, Performance change of a semi-submersible production platform system with broken mooring line or riser, Eng. Fail. Anal., 118 (2020) 104819, doi: 10.1016/j.engfailanal.2020.104819.
[18] H.Y. Wu, Y.S. Zhao, Y.P. He, Y.L. Shao, W.G. Mao, Z.L. Han, C. Huang, X.L. Gu, Z.Y. Jiang, Transient response of a TLP-type floating offshore wind turbine under tendon failure conditions, Ocean Eng., 220 (2021) 108486, doi: 10.1016/j.oceaneng.2020.108486.
[19] Y. Yang, M. Bashir, C. Li, J. Wang, Investigation on mooring breakage effects of a 5 MW barge-type floating offshore wind turbine using F2A, Ocean Eng., 233 (2021) 108887, doi: 10.1016/j.oceaneng.2021.108887.
[20] D.S. Qiao, B.B. Li, J. Yan, Y. Qin, H.Z. Liang, D.Z. Ning, Transient responses evaluation of FPSO with different failure scenarios

of mooring lines, J. Mar. Sci. Eng., 9 (2021) 103, doi: 10.3390/jmse9020103.
[21] H.T. Wu, L. Cui, W.X. Liu, Z.Y. Zhang, J.C. Kang, Performance changes of an engineering ship with one mooring line failure, Eng. Fail. Anal., 137 (2022) 106233, doi: 10.1016/j.engfailanal.2022.106233.
[22] Y.J. Ren, V. Venugopal, W. Shi, Dynamic analysis of a multi-column TLP floating offshore wind turbine with tendon failure scenarios, Ocean Eng., 245 (2022) 110472, doi: 10.1016/j.oceaneng.2021.110472.
[23] C.L. Zhang, S.M. Wang, S.Y. Xie, J. He, J. Gao, C.F Tian, Effects of mooring line failure on the dynamic responses of a semisubmersible floating offshore wind turbine including gearbox dynamics analysis, Ocean Eng., 245 (2022) 110478, doi: 10.1016/j.oceaneng.2021.110478.
[24] Q. Meng, Q. Ma, G. Zhou. Adaptive output feedback control for stochastic uncertain nonlinear time-delay systems, IEEE Trans. Circuits Syst. II Express Briefs, 69 (2022) 3289–3293.
[25] O.M. Faltinsen, Sea Loads on Ships & Offshore Structures, Cambridge University Press, 1993.
[26] M.N. Yue, Q.S. Liu, C. Li, Q.W. Ding, S.S. Cheng, H.T. Zhu, Effects of heave plate on dynamic response of floating wind turbine Spar platform under the coupling effect of wind and wave, Ocean Eng., 201 (2020) 107103, doi: 10.1016/j.oceaneng.2020.107103.
[27] T.S. Sarpkaya, Wave Forces on Offshore Structures, Cambridge University Press, United Kingdom, 2010.
[28] G. Xiao, B. Chen, S. Li, X. Zhuo, Fatigue life analysis of aero-engine blades for abrasive belt grinding considering residual stress, Eng. Fail. Anal., 131 (2022) 105846, doi: 10.1016/j.engfailanal.2021.105846.
[29] G.K. Batchelor, An Introduction to Fluid Dynamics, Cambridge University Press, 1967.
[30] C.Y. Ji, Y. Cheng, Q. Yan, G. Wang, Fully coupled dynamic analysis of a FPSO and its MWA system with mooring lines and risers, Appl. Ocean Res., 58 (2016) 71–82.
[31] Z.J. Chuang, S.W. Liu, C.Z. Li, Y. Lu, X. Chang, Dynamic analysis of semi-submersible production platform under the failure of mooring lines, China Ocean Eng., 35 (2021) 84–95.
[32] Q. Cao, L.F. Xiao, X.X. Guo, M.Y. Liu, Second-order responses of a conceptual semi-submersible 10 MW wind turbine using full quadratic transfer functions, Renewable Energy, 153 (2020) 653–668.
[33] L.X. Zhang, W. Shi, M. Karimirad, C. Michailides, Z.Y. Jiang, Second-order hydrodynamic effects on the response of three semisubmersible floating offshore wind turbines, Ocean Eng., 207 (2020) 107371, doi: 10.1016/j.oceaneng.2020.107371.
[34] B. Mou, Y. Bai, Experimental investigation on shear behavior of steel beam-to-CFST column connections with irregular panel zone, Eng. Struct., 168 (2018) 487–504.